12th International Symposium on Advanced Vehicle Control
September 22-26, 2014

AVEC '14

20149285

Collision Strength Estimation and Preemptive Steering Control for Post-Impact Vehicle Motion Control

Byung-joo Kim, Huei Peng
The University of Michigan

G041 Lay Auto Lab, University of Michigan
Ann Arbor, MI, 48109, USA
Phone: 1-734-647-9732
E-mail: bjukim@umich.edu

This study proposes a preemptive steering control strategy that takes into consideration post-impact vehicle stability. To reduce the risk of subsequent crashes after an initial impact, sufficiently fast decision and control are desired for stabilizing the vehicle motion. As opposed to active steering systems for lane or path tracking, the proposed control system needs to assess the strength of impact from the other vehicle and predict the resulting vehicle motion. To achieve faster and more effective control responses, impact prediction and estimation schemes that are performed before and at an early stage of a crash are proposed. Based on the predicted or estimated collision strength, a proper steering action is taken to drive the vehicle motion to a desired final state. Simulations and analysis results of the proposed estimation and prediction algorithm are presented, followed by the demonstration that shows the usefulness of the proposed steering control algorithm.

Topics / Active safety & Driver assistance systems, Vehicle collision avoidance, Vehicle dynamics

1. INTRODUCTION

Approximately 5.3 million motor vehicle crashes were reported during 2011 in the United States which resulted in about 32,500 fatalities [1]. Among them, about 40 % were the result of multiple vehicle crashes. Several statistical studies based on NASS-CDS (National Automotive Sampling System – Crashworthin -ess Data System) data [2-4] indicate that multiple impact crashes have increased. These reports found that the risk of severe injuries is much higher in multiple impact crashes than in single impact crashes. In [5], it is also pointed out that the risks of both injuries and fatalities increased with the number of collision events. It is also shown in [6] that harmful secondary impact crashes are often associated with high-speed crashes, because the vehicle's kinetic energy is relatively high and is more likely to sustain a subsequent impact after the first event. The initial impact typically startles the driver who then fails to maintain control. Since a loss of control leads to intense skidding and large lateral forces, more severe subsequent events are likely to occur. Moreover, because drivers usually pay more attention to the front than the side or back [7], typical drivers are not ready to react to unexpected side or rear collision from other vehicles. To consider vehicle motion induced by the initial collision and to stabilize the vehicle after the impact, several Post-Impact Stability Control (PISC) strategies have been proposed [8-11]. And, these studies show that control actions after an impact are important and effective to reduce the risk of subsequent events.

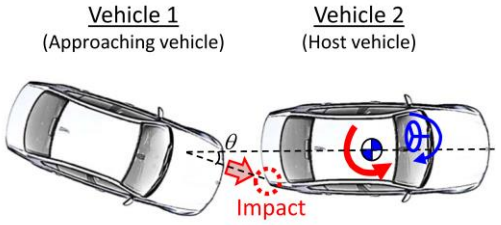

Fig. 1 A crash scenario showing a counter-steering control to negate the vehicle motion due to an impact

In this paper, we propose a preemptive vehicle stabilizing control concept considering vehicle impact, as shown in Fig. 1. Suppose that an active safety system can trace the positions and velocities of other vehicles from on-board or off-board sensors and detect an approaching vehicle (Vehicle 1), then generating a counter yaw moment, even before the collision event, is possible by applying a steering action in Vehicle 2. A major benefit of this action is to avoid large tire slip angles which renders differential braking ineffective. The proposed control algorithm will initiate just before or at the early stage of the collision. For this purpose, impact strength estimation and force prediction play an important role to determine the proper steering control magnitude. The remainder of this paper is organized as follows. Vehicle and tire models used in this study are presented in Section 2. Section 3 describes the collision model. The proposed control strategy is shown in Section 4. Simulation results in Section 5 are followed by conclusions in Section 6.

2. VEHICLE AND TIRE MODELS

2.1 Vehicle Model

The main interest regarding vehicle model in this research is on the characterization of changes in vehicle kinematic states due to the collision. Therefore, changes in planar vehicle motions are the major concern. The vehicle is commonly treated as a rigid body with three degrees of freedom (DOF) (longitudinal, lateral, and yaw). When the vehicle roll motion is not negligible, a 4-DOF model needs to be considered. In [12], it was pointed out that the vehicle roll motion should be considered to reduce the error in predicting vehicle lateral and yaw motions after a collision. The schematic diagram of the vehicle model is shown in Fig 2. This vehicle model separates the rolling (sprung) mass m_R from the non-rolling (unsprung) mass m_{NR}. The effect of the suspension elements at each corner is lumped into an equivalent torsional spring and a damper around the roll axis. The overall mass of the vehicle is denoted as *M*. The coordinate system $x-y-z$ is fixed on the vehicle body with the ISO coordinate convention. The roll axis (x-axis) passes through the non-rolling mass and is assumed to be parallel to the ground. The distance between the rolling mass CG (Center of Gravity) and the roll axis is denoted as h, whereas the height of the overall CG above the ground is denoted as h_{CG}.

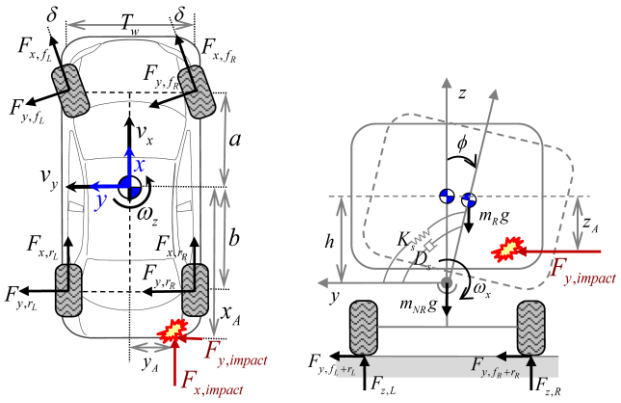

(a) Top view of the model (b) Rear view of the model

Fig. 2 Vehicle model with external impact forces

Fig. 2 also shows vehicle longitudinal velocity (v_x), lateral velocity (v_y), yaw rate (ω_z), roll angle (ϕ), and roll rate (ω_x) acting on CG located at a distance a and b from front and rear axles. The impact forces ($F_{x,impact}$, $F_{y,impact}$) are assumed to be acting along the horizontal plane. The impact position (A) is at (x_A, y_A, z_A). The dynamic equations are shown as follows:

Longitudinal motion

$$M(\dot{v}_x - v_y\omega_z) = F_{x,impact} + \left(F_{x,f_L} + F_{x,f_R}\right)\cos\delta - \left(F_{y,f_L} + F_{y,f_R}\right)\sin\delta + \left(F_{x,r_L} + F_{x,r_R}\right) \quad (1)$$

Lateral motion

$$M(\dot{v}_y + v_x\omega_z) - m_R h\dot{\omega}_x = F_{y,impact} + \left(F_{y,r_L} + F_{y,r_R}\right) + \left(F_{x,f_L} + F_{x,f_R}\right)\sin\delta + \left(F_{y,f_L} + F_{y,f_R}\right)\cos\delta \quad (2)$$

Yaw motion

$$I_{zz}\dot{\omega}_z + I_{xz}\dot{\omega}_x = x_A F_{y,impact} - y_A F_{x,impact} + a\left(F_{x,f_L} + F_{x,f_R}\right)\sin\delta + a\left(F_{y,f_L} + F_{y,f_R}\right)\cos\delta - b\left(F_{y,r_L} + F_{y,r_R}\right) + {T_W}/{2}\left(F_{xRR} - F_{xRL}\right) + {T_W}/{2}\left[\left(F_{x,f_R} - F_{x,f_L}\right)\cos\delta - \left(F_{y,f_R} - F_{y,f_L}\right)\sin\delta\right] \quad (3)$$

Roll motion

$$I_{xx,s}\dot{\omega}_x + I_{xz}\dot{\omega}_z - m_R h(\dot{v}_y + v_x\omega_z) = F_{y,impact}(z_A - h) + (m_R gh - K_s)\phi - D_s\omega_x \quad (4)$$

The vehicle yaw moment of inertia about the z-axis is denoted as I_{zz}. As parameters for roll motion, $I_{xx,s}$ is the roll moment of inertia of sprung mass with respect to the x-axis, I_{xz} is the product of inertia of the sprung mass about x- and z-axes, K_s and D_s are roll stiffness and damping coefficients of all suspensions.

2.2 Tire Model

The combined-slip Pacejka's Magic Formula (MF) model [13] is used in this study. This model uses empirically calibrated parameters to emulate the tire force profile for given slip ratio, slip angle, vertical load and the surface friction coefficient. The basic form of MF model is as follows:

$$\left[F_{x,tire} \quad F_{y,tire}\right]^T = P\left(\frac{C_\alpha \|s\|}{F_p(F_z)}, C, E\right)\cdot\frac{F_p(F_z)}{\|s\|}\cdot s \quad (5)$$

where,

$$P(\chi, C, E) = \sin\left[C\cdot\arctan\left\{\frac{\chi}{C} - E\left(\frac{\chi}{C} - \arctan\left(\frac{\chi}{C}\right)\right)\right\}\right] \quad (6)$$

$$s = \left[s_x \quad s_y\right]^T = \left[\lambda \quad \tan\alpha\right]^T \quad (7)$$

$$F_p(F_z) = F_z \Big/ \left(1 + \left(1.5\cdot\frac{F_z}{M\cdot g}\right)^3\right) \quad (8)$$

$$C_\alpha = c_1\cdot M\cdot g\cdot\left(1 - e^{-\frac{c_2\cdot F_z}{M\cdot g}}\right) \quad (9)$$

The parameters c_1 and c_2 are dimensionless constants obtained through data-fitting. And the cornering stiffness C_α changes with the tire normal load. In this study, road friction coefficient (μ) is assumed to be constant corresponding to a dry asphalt ($\mu = 0.7$). Fig. 3 shows the tire force profiles over the entire range of tire slip angle (α) and longitudinal slip ratio (λ). It should be noted that longitudinal and lateral tire forces vary nonlinearly along the tire slip angles. When α is near 0º, variations in slip ratio λ yield large changes in both longitudinal and lateral forces, meaning there is significant "control authority" in affecting tire forces. On the contrary, the effects of λ are small when α is around ±90º, meaning that control authorities become very limited.

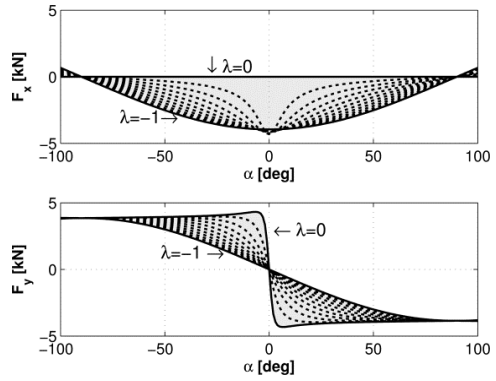

Fig. 3 Tire model showing longitudinal and lateral tire forces (Dotted lines are forces with $\lambda \in (-1,0)$)

The key innovation of this paper is to develop a preemptive steering control algorithm that reduces yaw motion with the purpose of preventing large tire slip angle, so that the subsequent differential braking control performance can be enhanced. Therefore, the proposed algorithm can be understood as an enabler to other differential-braking based post-impact control strategy presented in [10]-[11].

3. COLLISION MODEL

The overall process for collision force estimation is shown in Fig. 4. To achieve faster control response, the crash force prediction is performed after a threat is detected which is before the collision happens (Stage I). The estimation is carried out assuming that the approaching vehicle speed, vehicle mass, and the expected contact location are available from on-board and/or off-board sensors. Next step (Stage II) starts, once a crash occurs and is detected. The impulse strength is estimated using measurements from the on-board sensors. The first three time steps of impulse estimations are extrapolated to project the half-way point of the presumed crash duration ($\Delta T = 0.15s$). In Stage III, the estimated collision forces are updated with more accurate collision time duration.

3.1 Collision Force Prediction (Stage I)

The collision effect prediction starts immediately after a crash threat is detected, using the velocity information of both vehicles, the estimated vehicle mass, and the possible location of the collision. Using the conservation of momentum method with 'inelastic collision' assumption, the velocities of both vehicles just after impact is formulated as follows:

$$\begin{aligned} & M_1 \cdot v_1 + M_2 \cdot v_2 \\ & = (M_1 + M_2) \cdot v_f \end{aligned} \quad \Rightarrow \; v_f = \frac{M_1 \cdot v_1 + M_2 \cdot v_2}{M_1 + M_2} \qquad (10)$$

The subscripts 1 and 2 represent 'vehicle 1 and 2', and v_f is the final speed after collision. By assuming that the masses of the two cars are identical, Equation (10) is simplified to an average speed of both car speeds ($v_f \approx (v_1 + v_2)/2$). By applying this relationship in both x- and y-directions, the magnitudes of the final velocity components ($v_{f,x}, v_{f,y}$) are found.

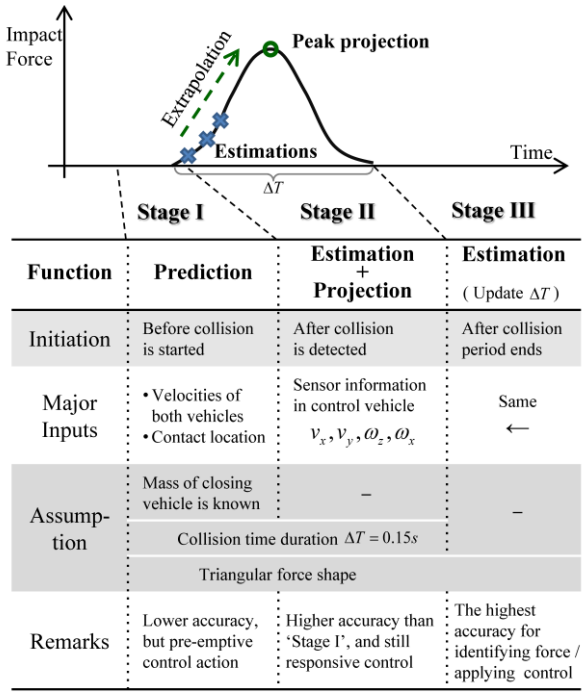

Function	Prediction	Estimation + Projection	Estimation (Update ΔT)
Initiation	Before collision is started	After collision is detected	After collision period ends
Major Inputs	• Velocities of both vehicles • Contact location	Sensor information in control vehicle $v_x, v_y, \omega_z, \omega_x$	Same ←
Assump-tion	Mass of closing vehicle is known	–	–
	Collision time duration $\Delta T = 0.15s$		
	Triangular force shape		
Remarks	Lower accuracy, but pre-emptive control action	Higher accuracy than 'Stage I', and still responsive control	The highest accuracy for identifying force / applying control

Fig. 4 Function descriptions of the three stages of collision force estimation

To calculate the impulse strength (the change in momentum before and after the collision), the linear momentum equations are used:

$$\Delta P_x = M \cdot (v_{f,x} - v_x), \; \Delta P_y = M \cdot (v_{f,y} - v_y) \qquad (11)$$

The strengths of the impulse are denoted as ΔP_x, ΔP_y. Since we only consider the motion of the control vehicle, subscript 1 is omitted for convenience. The "identical mass assumption" is adequate to start the control action. When better information is available, it certainly can be used for a more accurate estimation and control. Once the impulse strength is estimated, by assuming the collision forces have triangular shape, the overall collision force profiles are predicted. As shown in Fig. 5, the base of the triangle is the collision time duration (ΔT). Since the typical time duration for a collision is around 0.1-0.2 seconds [14], the presumed time duration in Stage I and II is set to 0.15 seconds. And, the duration will be updated in Stage III using transient vehicle motion information acquired from sensors.

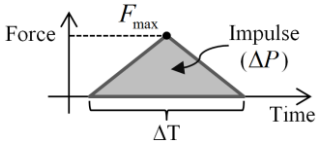

Fig. 5 Approximated impact force profile

3.2 Impulse Strength Estimation and Projection (Stage II)

Using vehicle sensor information, the magnitude and the location of the impulse can be computed by using a crash dynamic model and the measured vehicle states. According to the relationship between impulse and force ($\Delta P_i = \int_{t_1}^{t_2} F_i dt$, $i = x, y$), the impulses are

derived by the integral forms of Equation (1)-(3). To simplify the equation, it is assumed that the steering angle and the longitudinal tire forces are small enough to ignore. The model includes the equations of motion in the longitudinal, lateral, and yaw degrees of freedom, presented in discrete time forms as follows [12]:

$$\begin{aligned}\Delta P_x &= M\cdot\left(v_{x,t}-v_{x,t-\Delta t}\right)\\ &\quad -M\frac{\Delta t}{2}\left(v_{y,t}\cdot\omega_{z,t}+v_{y,t-\Delta t}\cdot\omega_{z,t-\Delta t}\right)\end{aligned} \tag{12}$$

$$\begin{aligned}\Delta P_y &= M\cdot\left(v_{y,t}-v_{y,t-\Delta t}\right)-m_R h\cdot\left(\omega_{x,t}-\omega_{x,t-\Delta t}\right)\\ &\quad +M\frac{\Delta t}{2}\left(v_{x,t}\cdot\omega_{z,t}+v_{x,t-\Delta t}\cdot\omega_{z,t-\Delta t}\right)\\ &\quad -\frac{\Delta t}{2}C_{\alpha,f}\left(\frac{v_{y,t}+a\cdot\omega_{z,t}}{v_{x,t}}+\frac{v_{y,t-\Delta t}+a\cdot\omega_{z,t-\Delta t}}{v_{x,t-\Delta t}}\right)\\ &\quad -\frac{\Delta t}{2}C_{\alpha,r}\left(\frac{v_{y,t}-b\cdot\omega_{z,t}}{v_{x,t}}+\frac{v_{y,t-\Delta t}-b\cdot\omega_{z,t-\Delta t}}{v_{x,t-\Delta t}}\right)\end{aligned} \tag{13}$$

$$\begin{aligned}&\Delta P_y x_A-\Delta P_x y_A=\\ &\quad I_{zz}\left(\omega_{z,t}-\omega_{z,t-\Delta t}\right)+I_{xz}\left(\omega_{x,t}-\omega_{x,t-\Delta t}\right)\\ &\quad -\frac{\Delta t}{2}aC_{\alpha,f}\left(\frac{v_{y,t}+a\cdot\omega_{z,t}}{v_{x,t}}+\frac{v_{y,t-\Delta t}+a\cdot\omega_{z,t-\Delta t}}{v_{x,t-\Delta t}}\right)\\ &\quad +\frac{\Delta t}{2}bC_{\alpha,r}\left(\frac{v_{y,t}-b\cdot\omega_{z,t}}{v_{x,t}}+\frac{v_{y,t-\Delta t}-b\cdot\omega_{z,t-\Delta t}}{v_{x,t-\Delta t}}\right)\end{aligned} \tag{14}$$

Note that the trapezoidal rule is used with a fixed time step (Δt) for the approximate integration of nonlinear terms ($v_y\omega_z$, $v_x\omega_z$, v_y/v_x , ω_z/v_x). The variables on the right-hand sides of Equations (12)-(14) are all assumed to be known from both the sensor measurements and vehicle parameters. The impact location in the $x-y$ plane is denoted as x_A, y_A. The subscripts for time (t and $t-\Delta t$) indicate different time steps. The cornering stiffness ($C_{\alpha,f}, C_{\alpha,r}$) values vary with the tire slip angles. Since the collision impact dramatically changes the tire slip angles, the linear relationship between the slip angle and the tire force is no longer accurate in high slip angle regions. To capture the nonlinearities of the tire force in Equations (13) and (14), an effective factor (η) is introduced to adjust the slope of the cornering stiffness as follows:

$$\eta_i(\alpha,\lambda)=-\frac{F_{y,i}(\alpha,\lambda)}{C_{\alpha,i}\cdot\alpha},\quad i\in\{\text{front, rear}\} \tag{15}$$

The value η can vary between zero and one. When the slip angle α is close to 90 degrees, the value η approaches zero. Once η is calculated and stored as a table varying with α and λ , all the nonlinearity of the tire lateral force can be considered using a modified cornering stiffness ($\eta\cdot C_{\alpha,i}$).

The projected peak force is assumed to occur at the half-way point of presumed crash duration ($\Delta T/2$) in Fig. 5. Since the magnitude of impulse is the area under the force profile, the impulse amount up to $\Delta T/2$ is the half area of the triangle. Then, the maximum forces ($F_{x,\max}, F_{y,\max}$) are calculated from the following equations:

$$F_{x_{\max}}=2\cdot\Delta P_{x_{\Delta T/2}}/\left(\frac{\Delta T}{2}\right),\quad F_{y_{\max}}=2\cdot\Delta P_{y_{\Delta T/2}}/\left(\frac{\Delta T}{2}\right) \tag{16}$$

3.3 Collision Time Duration Update (Stage III)

The end of a collision is detected using sensors and impulse estimation results. If the estimated impulse stops changing or the sensor measurements no longer show impulsive results, they can be used to indicate the end of the collision. In this way, the force projection based on a presumed time duration ($\Delta T=0.15s$) is updated with a more accurate time duration. Since the force projection is conducted based on the slope at the beginning of the collision, different amount of force can be predicted depending on the time duration, as shown in Fig. 6. In fact, the relative error in areas under the triangular profile can be, at most, 50~70%. For this reason, the presumed time duration ($\Delta T=0.15s$) needs to be updated to correct the collision force estimation.

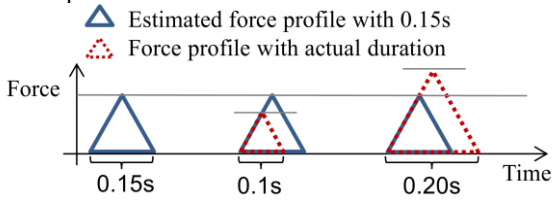

Fig. 6 Force levels with different crash time durations

4. CONTROLLER DESIGN

The steering action changes the vehicle lateral and yaw motion. As shown in Fig. 7, the converging point on the $\beta-\omega_z$ phase plane with a steering angle is not the origin. So, the resulting yaw rate due to an impact can be reduced because the opposite directional yaw rate is developed in advance through the steering action. In addition, the steering mitigates large sideslip angle development with relatively faster yaw rate reduction.

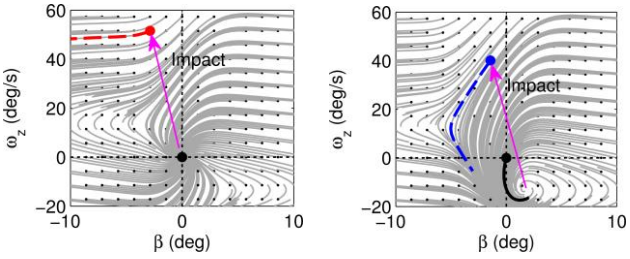

(a) $\delta=0^\circ$ (b) $\delta=-2.5^\circ$

Fig. 7 Vehicle motion on the phase plane with v_x =30 m/s (Each dot represents an initial condition and each gray line is propagated vehicle motion traces from the dot). An impact, which causes $\Delta\omega_z=50^\circ/s$, $\Delta\beta=-3^\circ$, applied when (a) neutral steering, and (b) -2.5° steering.

The designed system monitors vehicles in the adjacent lanes and behind the host vehicle. When a motion of a vehicle around the host vehicle is assessed as an imminent collision, the system applies steering torque to generate a counter yaw moment against the

impact force. The impact position and angle information is assumed to be available from a sensor. The force prediction and estimation procedure presented in Chapter 3 play major roles in determining a feedforward control input. For this reason, the effectiveness of the feedforward controller depends on the accuracy of force prediction or estimation. While significant vehicle motion may still develop during and after an impact, a feedback controller starts to take action to attenuate the vehicle motions that were not cancelled by the feedforward action. As shown in Fig. 8, the final desired steering commands is the sum of feedforward and feedback control actions.

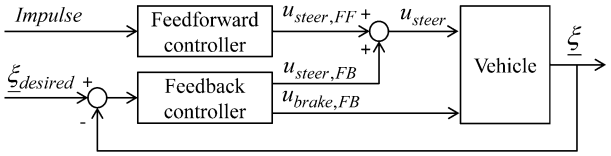

Fig. 8 Block diagram of the control structure, $\underline{\xi} = [v_y \ \omega_z]^T$

3.1 Feedforward Controller

The purpose of the feedforward loop is to achieve faster vehicle motion response which alleviates the collision effect preemptively. So, the steering angle is determined by the expected vehicle motion after the impact. The vehicle motion can be predicted by using the vehicle model in Equation (1)-(4). The impact forces in this prediction are triangle profiles with Equation (16). Then the target yaw motion with the steering control is set to cancel the predicted vehicle motion with the perceived impact disturbance. The mathematical relationship between steering control angle (δ) and target vehicle yaw rate ($\omega_{z,\text{target}}$) is expressed by the Ackerman angle [15]:

$$\delta = \left\{ \frac{(a+b)}{v_x} + K_u \cdot v_x \right\} \cdot \omega_{z,\text{target}} \tag{17}$$

where, $K_u = -\frac{M}{a+b} \cdot \left\{ \frac{a}{C_{\alpha,r}} - \frac{b}{C_{\alpha,f}} \right\}$

The structure of the feedforward control block is shown in Fig. 9.

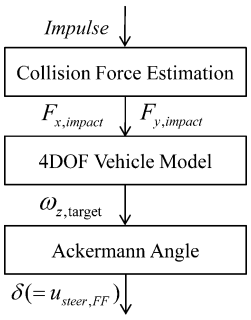

Fig. 9 Feedforward control block structure

3.2 Feedback Controller

The feedback controller is designed by using the planar 3-DOF vehicle model which excludes the roll motion and external forces in Equation (2) and (3). Then the lateral and yaw dynamics equations of motions of the vehicle are:

$$\begin{aligned} M \cdot (\dot{v}_y + v_x \omega_z) = & \left(F_{x,f_L} + F_{x,f_R}\right)\sin\delta \\ & + \left(F_{y,f_L} + F_{y,f_R}\right)\cos\delta + \left(F_{y,r_L} + F_{y,r_R}\right) \end{aligned} \tag{18}$$

$$\begin{aligned} I_{zz}\dot{\omega}_z = & a\left(F_{x,f_L} + F_{x,f_R}\right)\sin\delta + a\left(F_{y,f_L} + F_{y,f_R}\right)\cos\delta \\ & - b\left(F_{y,r_L} + F_{y,r_R}\right) + \frac{T_W}{2}\left(F_{x,r_R} - F_{x,r_L}\right) \\ & + \frac{T_W}{2}\left[\left(F_{x,f_R} - F_{x,f_L}\right)\cos\delta - \left(F_{y,f_R} - F_{y,f_L}\right)\sin\delta\right] \end{aligned} \tag{19}$$

In order to keep considering nonlinearities and stabilize the system from the disturbance, the sliding mode control concept is applied. Since the purpose of the control is designed to bring both lateral velocity and yaw rate to the desired states ($v_{y,d}$, $\omega_{z,d}$), the multiple sliding surface control theory [11, 16] is applied to suppress those output errors. The first and the second sliding surfaces are defined as

$$S_1 = v_y - v_{y,d} \tag{20}$$

$$S_2 = \omega_z - \omega_{z,d} \tag{21}$$

To achieve control objectives, it is desired that

$$\dot{S}_1 = -k_1 \cdot S_1 \tag{22}$$

$$\dot{S}_2 = -k_2 \cdot S_2 \tag{23}$$

where, k_1 and k_2 are positive definite values which can be chosen for the convergence rate of the control. Then the sliding surfaces yield the following lateral and yaw accelerations:

$$\dot{v}_y = \dot{v}_{y,d} - k_1 \cdot \left(v_y - v_{y,d}\right) \tag{24}$$

$$\dot{\omega}_z = \dot{\omega}_{z,d} - k_2 \cdot \left(\omega_z - \omega_{z,d}\right) \tag{25}$$

Substituting the relationship in Equation (24) into (18) and rearranging yields the desired vehicle yaw rate ($\bar{\omega}_{z,d}$) for the first sliding surface:

$$\begin{aligned} \bar{\omega}_{z,d} = & \frac{\left(\hat{F}_{x,f_L} + \hat{F}_{x,f_R}\right)\sin\delta + \left(\hat{F}_{y,f_L} + \hat{F}_{y,f_R}\right)\cos\delta}{M \cdot v_x} \\ & + \frac{\hat{F}_{y,r_L} + \hat{F}_{y,r_R}}{M \cdot v_x} - \frac{\dot{v}_{y,d} - k\left(v_y - v_{y,d}\right)}{v_x} \end{aligned} \tag{26}$$

Here, we assume that a tire force estimator for both longitudinal and lateral directions exists and its accuracy is high enough. The estimated values are marked with "^" symbol. The yaw rate command in Equation (26) is processed with a first-order filter to feed into the second sliding surface.

$$\tau \cdot \dot{\omega}_{z,d} + \omega_{z,d} = \bar{\omega}_{z,d} \tag{27}$$

where, τ is the time constant for the filter.

As feedback control inputs, two types of actuators that generate yaw moment to the vehicle are considered: a front tire steering angle and a yaw moment by independent tire braking forces:

$$u_1 = \delta \tag{28}$$

$$\begin{aligned} u_2 = & \frac{T_W}{2}\left[\left(F_{x,f_R} - F_{x,f_L}\right)\cos\delta + \left(F_{x,r_R} - F_{x,r_L}\right)\right] \\ & + a\left(F_{x,f_L} + F_{x,f_R}\right)\sin\delta \end{aligned} \tag{29}$$

Substituting Equation (29) into (19) and adding a small steering angle assumption result in following expression:

$$\dot{\omega}_z = \frac{1}{I_{zz}}u_2 - \frac{b}{I_{zz}}\left(F_{y,r_L} + F_{y,r_R}\right) + \frac{a}{I_{zz}}\left(F_{y,f_L} + F_{y,f_R}\right) - \frac{T_W}{2\cdot I_{zz}}\left(F_{y,f_R} - F_{y,f_L}\right)\cdot u_1 \quad (30)$$

Using Equation (25) and rearranging the terms in Equation (30), we have the desired steering angle and the desired yaw moment using brakes as feedback controls ($u_{steer,FB}$, $u_{brake,FB}$):

$$u_{steer,FB} = \frac{-2}{T_W\cdot\left(\hat{F}_{y,f_R} - \hat{F}_{y,f_L}\right)}\cdot \left[\begin{array}{l} b\left(\hat{F}_{y,r_L} + \hat{F}_{y,r_R}\right) - a\left(\hat{F}_{y,f_L} + \hat{F}_{y,f_R}\right) - \hat{u}_2 \\ +I_{zz}\cdot\left\{\dot{\omega}_{z,d} - k_2\left(\omega_2 - \omega_{z,d}\right)\right\}\end{array}\right] \quad (31)$$

$$u_{brake,FB} = -a\cdot\left(\hat{F}_{y,f_L} + \hat{F}_{y,f_R}\right) + b\cdot\left(\hat{F}_{y,r_L} + \hat{F}_{y,r_R}\right) + \frac{T_W}{2}\cdot\left(\hat{F}_{y,f_R} - \hat{F}_{y,f_L}\right)\cdot\hat{u}_1 + I_{zz}\cdot\left\{\dot{\omega}_{z,d} - k_2\left(\omega_2 - \omega_{z,d}\right)\right\} \quad (32)$$

The desired yaw moment is converted into variations of brake forces at each wheel, and applying either the left or right side brakes is decided by the direction of the desired yaw moment. Then Equation (32) can be divided into two cases:

When $u_{brake,FB} > 0$,

$$u_{brake,FB} = \left(-\frac{T_W}{2}\cos\delta + a\sin\delta\right)F_{x,f_L} - \frac{T_W}{2}F_{x,r_L} \quad (33)$$

When $u_{brake,FB} < 0$,

$$u_{brake,FB} = \left(\frac{T_W}{2}\cos\delta + a\sin\delta\right)F_{x,f_R} + \frac{T_W}{2}F_{x,r_R} \quad (34)$$

The braking control pressure amounts are approximated by the linear relationship between wheel brake pressure and corresponding braking force. Then the desired yaw moment has a relationship with braking pressure (P) as

$$u_{brake,FB} = \kappa_f\cdot P_{f_{L\ or\ R}} + \kappa_r\cdot P_{r_{L\ or\ R}} \quad (35)$$

where, κ_f and κ_r are linearized constant gains.

To determine the front and rear wheel brake pressure, a brake proportioning rule is followed:

$$P_{r_L} = \rho\cdot P_{f_L},\ P_{r_R} = \rho\cdot P_{f_R} \quad \text{where, } \rho\in(0,1) \quad (36)$$

5. SIMULATION RESULTS

In this section, the system effectiveness is verified through the commercial vehicle dynamics software Carsim [17] and Simulink simulations for an angled rear-end collision scenario. Vehicle parameters are set to the "baseline big SUV" dataset in CarSim as detailed in Table 1. It is assumed that the vehicle travels straight with a speed of 30 m/s with no initial lateral speed, yaw rate, and roll rate before the impact. The impact is assumed to be located at 0.1 m to the right on the rear bumper and 0.66m height above the ground. In Fig. 10, the dynamic responses of 4-DOF model are compared to those of Carsim model.

Table 1 Parameters for vehicle model

Parameter	Symbol	Value
Total vehicle mass	M	2450 kg
Rolling mass	m_R	2210 kg
Non-rolling mass	m_{NR}	240 kg
Distance from axles to vehicle CG	a, b	1.105, 1.745 m
Distance from sprung mass CG to the roll axis	h	0.40 m
Vehicle yaw moment of inertia about z axis	I_{zz}	4946 kg·m^2
Sprung mass product of inertia about roll and yaw axes	I_{xz}	40 kg·m^2
Sprung mass roll moment of inertia about the roll axis	I_{xxs}	1597 kg·m^2
Total suspension roll stiffness	K_s	94000 N·m/rad
Total suspension roll damping	D_s	8000 N·m·s/rad

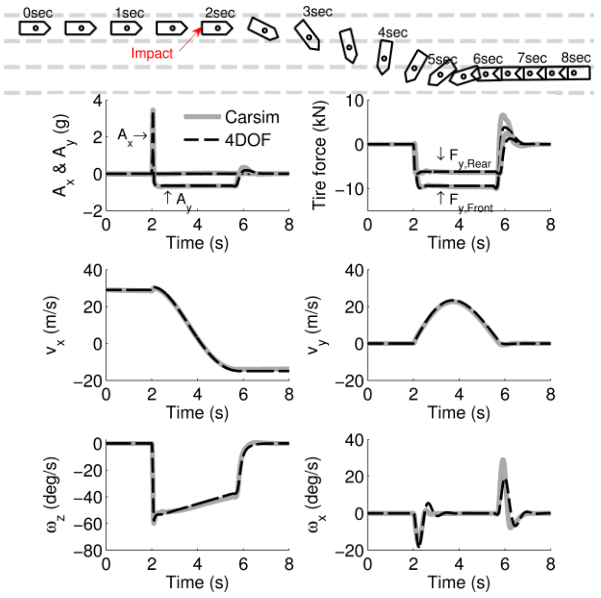

Fig. 10 Vehicle model response validation (No control action is involved. Initial speed: $v_x = 30$m/s)

The impact at 2 seconds has a strength which shows a maximum acceleration of 3.7g (Ax=3.4g, Ay=1.4g). Although there are small differences in roll rate and tire forces, a sufficiently close agreement between these two sets of responses are shown. The proposed impulse estimation and collision force prediction algorithms are validated in Fig. 11. The haversine shape external forces are applied to the simulation model. Estimated impulse points are marked with crosses. Since the collision duration (ΔT) is presumed to be 0.15 seconds, the projected impulse is marked at 2.075 seconds. The predicted forces are obtained by calculating Equation (16). The result shows that the projected triangle force shapes are fairly close to the actual ones.

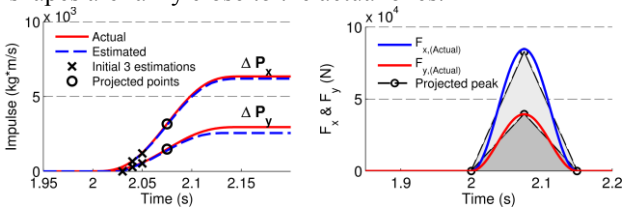

(a) (b)

Fig. 11 Comparison of actual and projected impulse and impact forces: (a) Collision impulses, (b) Collision forces

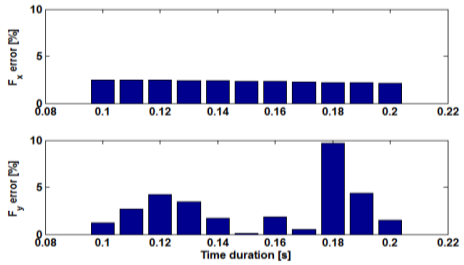

Fig. 12 Collision estimation errors

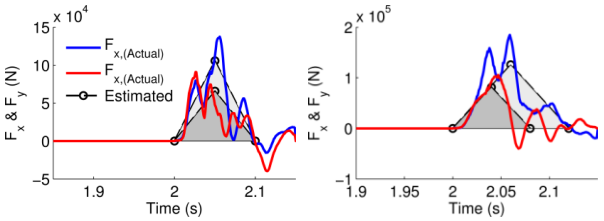

(a) (b)

Fig. 13 Comparison with experimental crash data NHTSA crash test no.: (a) v04667, (b) v04955

Similar simulation test were conducted to check the estimation performance with different collision time durations. For quantitative comparisons, areas under the force curves are examined. Fig. 12 gives the force estimation area errors along the range of collision time durations from 0.1 seconds to 0.2 seconds. The overall area errors between the actual and the predicted ones are shown within a range of 10%. The proposed algorithm is also validated with real collision experimental data from the NHTSA Crash Test Database [18]. To consider the initial impact condition leading to vehicle rotational and lateral motion, some of frontal offset tests were chosen for the algorithm validation. For comparison, estimated simulations results are overlapped with the two different experimental data as shown in Fig. 13. Overall, the projected force areas are fairly close to the actual force areas. Area errors between the predicted forces and the actual forces are under 5%. Then, vehicle motion prediction is performed using the estimated forces, as shown in Fig. 14.

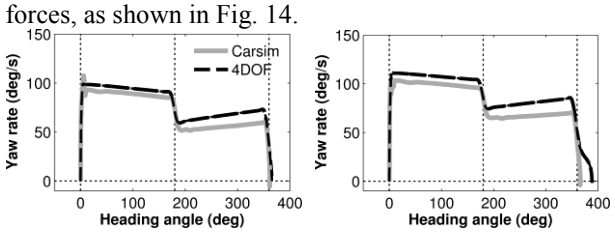

(a) (b)

Fig. 14 Vehicle motion prediction results with experimental force data in Fig. 11

The simulation test results shown in Fig (15)-(18) demonstrate the feasibility of this preemptive steering control action. It is assumed that the vehicle that violates a lane and causes a collision has a different angle from traveling axes (25°) when the collision occurs with a speed of 33.5 m/s (120 km/h or 75 mph) speed. The vehicles being struck run straight along the road with 30 m/s (108 km/h or 67 mph) speed. As a proposed control, counter yaw rate is generated 0.5 seconds before the collision event which significantly reduces the effect of vehicle motion due to the impact. On the other hand, the vehicle without control shows a large lateral deviation from its course and a substantial slip angle develops as shown in Fig. 15. It is also noted that the steering and braking control after the impact (PISC) shows relatively larger lateral deviation than the proposed control. Fig. 16 shows the time history comparisons of motion variables. The collision impact generates -1.1 g lateral peak acceleration and 51 °/s peak yaw rate without a control intervention and causes a large lateral deviation and sideslip angle.

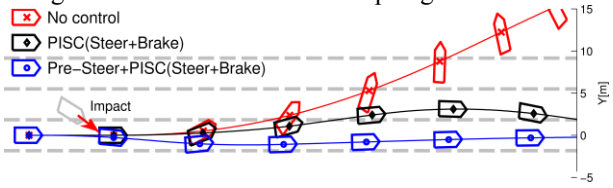

Fig. 15 Trajectories of the vehicles under imposing an impact forces with a vehicle to vehicle collision

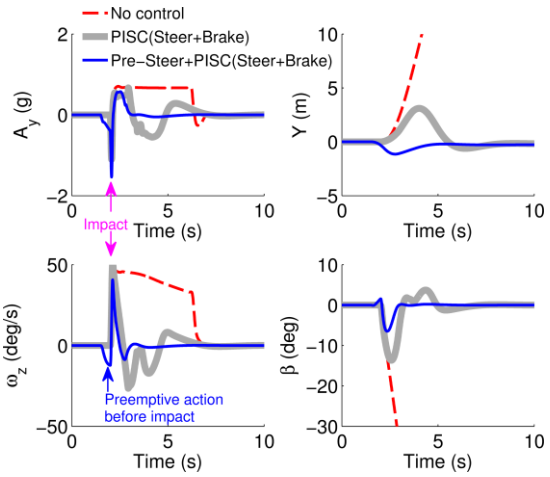

Fig. 16 Test result comparison. (vehicle motion without control, with a steering and brake control during and after the impact (PISC), and with preemptive counter-steering control before the impact)

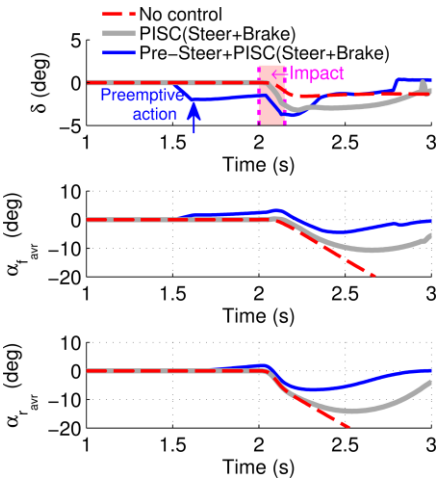

Fig. 17 Tire slip angle comparisons with wheel steering angle actions under an impact condition ($\alpha_{f_{avr}}, \alpha_{r_{avr}}$: average slip angles of front two tires and rear two tires)

The preemptive steering control is triggered at 1.95 seconds, which results in -0.39 g lateral acceleration and -12 °/s yaw rate right before the impact (2.0-2.15 seconds). Note that the direction of yaw rate from the steering action and the direction of the yaw rate from the impact are opposite. From this control, the yaw rate and the sideslip angle converge to zero with less oscillation than that of PISC. The wheel steering control outputs are shown in Fig. 17. It is noted that the proposed system reduces both front and rear tire slip angles. Considering that the control authority of steering and braking can be dramatically reduced when the tire is saturated, keeping the tire slip angle as small as possible is beneficial for the following control sequence.

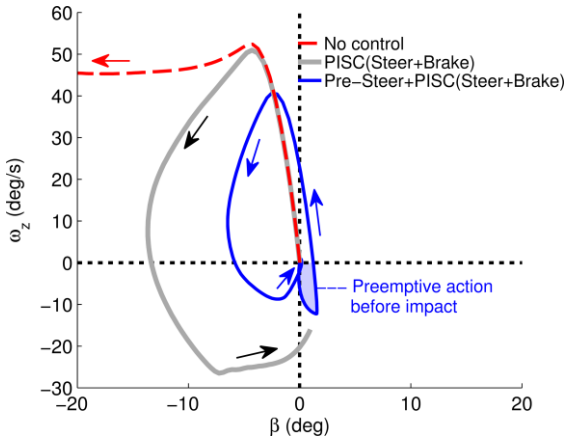

Fig. 18 Evolution of the vehicle motion trajectories on the slip angle-yaw rate phase plane ($\beta - \omega_z$) under an impact condition

With a phase plane view in Fig. 18, it is also obvious that the proposed control system suppresses the yaw and sideslip motion and improves the convergence rate to the origin in vehicle motion. These results show that the subsequent control performances after the preemptive action become much effective when the preemptive control suppress the large tire slip angles and yaw motion against a collision impact.

6. CONCLUSION

This paper proposes a preemptive steering control strategy with assessing collision strength. The collision force estimation algorithm is developed based on a 4-DOF vehicle model. The steering control, as a counter-steering action, is designed with feedforward and feedback controller to attenuate the vehicle motion due to an impact. The performance of the proposed algorithm is verified in impact force estimations and vehicle motion predictions. The algorithm also validated with a realistic crash data. Finally, it is shown that the preemptive steering control can stabilize the vehicle effectively with small tire slip angles, which results in a small lateral deviation from the original trajectory. Moreover, the proposed control algorithm can potentially be implemented for a driver assistance system such as the Blind Spot Detection system [19, 20] and extend its functionality to enhance driving safety.

REFERENCES

[1] NHTSA, "Traffic Safety Facts," US Department of Transportation 2011.
[2] Bahouth, J. and Digges, K. "Characteristics of multiple impact crashes that produce serious injuries," in 19th ESV, 2005.
[3] Sander, U. et al., "The effect of pre-pretensioning in multiple impact crashes," in 21st International Technical Conference on the Enhanced Safety of Vehicles (ESV), 2009.
[4] Togawa, A. et al., "An insight into multiple impact crash statistics to search for future directions of counter-approaches," in 22nd International Technical Conference on the Enhanced Safety of Vehicles (ESV), 2011.
[5] Zhou, J. "Active safety measures for vehicles involved in light vehicle-to-vehicle impacts," Ph.D., Mechanical Engineering, The University of Michigan, 2009.
[6] Eigen, A. and Najm, W. "Problem definition for pre-crash sensing advanced restraints," DOT HS, vol. 811, 2009, p. 114.
[7] Ayres, T. et al., "Passenger-side rear-view mirrors: driver behavior and safety," International journal of industrial ergonomics, vol. 35, 2005, pp. 157-162.
[8] Chan, C., and Tan, H. "Feasibility analysis of steering control as a driver-assistance function in collision situations," Intelligent Transportation Systems, IEEE Trans. on 2.1, 2001, pp. 1-9.
[9] Robert Bosch GmbH. "Secondary Collision Mitigation," available from http://www.bosch.com
[10] Yang, D. et al., "Post-impact vehicle path control by optimization of individual wheel braking sequences," Proc. of AVEC 2010, pp. 882-887.
[11] Zhou, J. et al., "Vehicle stabilization in response to exogenous impulsive disturbances to the vehicle body," in American Control Conference, 2009, pp. 701-706.
[12] Zhou, J. et al., "Collision model for vehicle motion prediction after light impacts," Vehicle System Dynamics, vol. 46, 2008, pp. 3-15.
[13] Pacejka, H. Tire and vehicle dynamics: Elsevier, 2005.
[14] Brach, R. "Modeling of low-speed, front-to-rear vehicle impacts," SAE Tech. 2003-01-0491, 2003.
[15] Rajamani, R. *Vehicle dynamics and control*. Springer, 2011.
[16] Hedrick, J. and Yip, P. "Multiple sliding surface control: theory and application," ASME Journal of Dynamic Systems, Measurement and Control, 122, 2000, pp. 586–593.
[17] Mechanical Simulation Corporation, available from: http://www.carsim.com]
[18] NHTSA. Crash Test Database, available from http://www-nrd.nhtsa.dot.gov/database/ veh/veh.htm
[19] Eidehall, A., et al. "Toward autonomous collision avoidance by steering," Intelligent Transportation Systems, IEEE Trans. on 8.1, 2007, pp.84-94.
[20] Jung, H. G., et al. "Isrss: Integrated side/rear safety system," International Journal of Automotive Technology on 11.4, 2010, pp. 541-553.